IEICE TRANS. FUNDAMENTALS, VOL.E100–A, NO.7 JULY 2017

LETTER

Robust Widely Linear Beamforming via an IAA Method for the Augmented IPNCM Reconstruction

Jiangbo LIU[†], ***Nonmember***, **Guan GUI**[††a)], ***Member***, **Wei XIE**[†], **Xunchao CONG**[†], **Qun WAN**[†b)], ***Nonmembers***, ***and*** **Fumiyuki ADACHI**[†††c)], ***Fellow***

SUMMARY Based on the reconstruction of the augmented interference-plus-noise (IPN) covariance matrix (CM) and the estimation of the desired signal's extended steering vector (SV), we propose a novel robust widely linear (WL) beamforming algorithm. Firstly, an extension of the iterative adaptive approach (IAA) algorithm is employed to acquire the spatial spectrum. Secondly, the IAA spatial spectrum is adopted to reconstruct the augmented signal-plus-noise (SPN) CM and the augmented IPNCM. Thirdly, the extended SV of the desired signal is estimated by using the iterative robust Capon beamformer with adaptive uncertainty level (AU-IRCB). Compared with several representative robust WL beamforming algorithms, simulation results are provided to confirm that the proposed method can achieve a better performance and has a much lower complexity.

key words: *widely linear beamforming, iterative adaptive approach, interference covariance matrix reconstruction, iterative robust Capon beamformer, signal steering vector estimation*

1. Introduction

As a fundamental technique in array signal processing, adaptive beamforming has been widely used in radar, sonar and wireless communications [1]. Conventional beamforming algorithms have mainly considered a time-invariant (TI) and linear complex filter for stationary observations, whose complex envelopes have been proved to be necessarily second-order (SO) circular [2]. However, SO noncircular signals are usually encountered in the context of radio communication or satellite communication, such as binary phase-shift keying (BPSK), unbalanced quaternary phase shift keying (UQPSK), and amplitude modulated (AM). In order to fully exploit the noncircular properties of the signals, many widely linear (WL) adaptive beamforming algorithms have been proposed in the last ten years, such as the WL minimum variance-based algorithm [3]–[6], the shrinkage adaptive filter-based algorithm [7], [8], and the noncircularity coefficient estimation-based algorithm [9]–[12]. The optimal WL minimum variance distortionless response (MVDR) beamformer was first proposed in [4], and its super performance was analyzed by Chevalier et al. in [5], [6]. Meanwhile, in order to achieve the optimal WL MVDR beamformer, the steering vector (SV) and the noncircularity coefficient of the desired signal should be known precisely. However, in a practical application, the accurate SV and the precise noncircularity coefficient of the desired signal are unavailable. To address this problem, some robust WL beamforming algorithms have been proposed in [8], [10], [12]–[15]. In [13], Wang's method can deal with the uncertainties in the desired signal's SV and noncircularity coefficient, but it is sensitive to the large mismatch of noncircularity coefficient. In [14], a robust WL beamformer based on a projection constraint was proposed. Wen et al. have proposed the noncircular robust Capon beamformer (NC RCB) in [10] to exploit the SO noncircularity of interferences and the desired signal simultaneously. However, it suffers severely from performance degradation at high signal-to-noise ratio (SNR). In [12], a robust WL beamforming algorithm based on the spatial spectrum of noncircularity coefficient was proposed by Xu et al. In [15], Huang et al. proposed two WL-minimum dispersion based beamforming algorithms to make full use of the noncircularity and sub-Gaussian properties of signals. Be aware that the robust WL beamformers in [12]–[15] are only limited in theory development rather than practical engineering field due to the high requirement of computational cost.

In this letter, we propose a new low complexity robust WL beamformer based on the techniques of the iterative adaptive approach (IAA) [16] and the iterative robust Capon beamformer with adaptive uncertainty level (AU-IRCB) [17]. Firstly, different from the IAA algorithm [16], we determine the positions of interferences first and then adopt the IAA algorithm to obtain the spatial spectrum. Secondly, the augmented interference-plus-noise (IPN) covariance matrix (CM) is reconstructed based on the acquired spatial spectrum. Thirdly, for noncircular signals, a modified AU-IRCB algorithm is developed to estimate the extended SV of the desired signal. Simulation results demonstrate that the proposed beamformer has a better performance than the beamformers in [10], [12], [15].

Notation: Matrices and vectors are denoted by boldface uppercase letters and boldface lowercase letters, respectively. $E\{\cdot\}$ denotes the expectation operator and $\|\cdot\|$ denotes the Euclidean norm. $(\cdot)^H$, $(\cdot)^T$ and $(\cdot)^*$ denote the conjugate transpose, the transpose and the complex conjugate, respectively. $\langle\cdot\rangle$ denotes the time-averaging operation.

Manuscript received November 30, 2016.
Manuscript revised March 8, 2017.
[†]The authors are with UESTC, Chengdu 611731, China.
[††]The author is with NUPT, Nanjing 210003, China.
[†††]The author is with Tohoku University, Sendai-shi, 980-8577 Japan.
a) E-mail: guiguan@njupt.edu.cn
b) E-mail: wanqun@uestc.edu.cn (Corresponding author)
c) E-mail: adachi@ecei.tohoku.ac.jp
DOI: 10.1587/transfun.E100.A.1562

2. The Signal Model

Considering an array with N narrowband sensors, the received signal can be represented by

$$\mathbf{x}(t) = s_0(t)\mathbf{a}_0 + \mathbf{v}(t), \tag{1}$$

where t is the time index, $\mathbf{v}(t) = \sum_{k=1}^{K} s_k(t)\mathbf{a}_k + \mathbf{n}(t)$ denotes the total IPN vector, K is the number of interferences and $\mathbf{n}(t)$ is the noise vector, $s_k(t)$ $(k = 0, 1, \cdots, K)$ represents the k-th signal complex waveform. $\mathbf{a}_0$ and $\mathbf{a}_k$ $(k = 1, 2, \cdots, K)$ are the true SVs of the desired signal and the k-th interference, respectively. The SO statistics of $\mathbf{x}(t)$ are given by

$$\mathbf{R}_x \triangleq \langle E[\mathbf{x}(t)\mathbf{x}(t)^H]\rangle = \pi_s\mathbf{a}_0\mathbf{a}_0^H + \mathbf{Q}_r, \tag{2}$$

$$\mathbf{C}_x \triangleq \langle E[\mathbf{x}(t)\mathbf{x}(t)^T]\rangle = \gamma_s\pi_s\mathbf{a}_0\mathbf{a}_0^T + \mathbf{Q}_c, \tag{3}$$

where $\mathbf{Q}_r = \langle E[\mathbf{v}(t)\mathbf{v}(t)^H]\rangle$, and $\mathbf{Q}_c = \langle E[\mathbf{v}(t)\mathbf{v}(t)^T]\rangle$. $\pi_s = \langle E[|s_0(t)|^2]\rangle$ and $\gamma_s = \langle E[s_0(t)^2]\rangle/\pi_s = |\gamma_s|e^{j\phi_s}$ are the desired signal's time-averaged power and noncircularity coefficient, respectively. For the desired noncircular signal with $|\gamma_s| \neq 0$, $s_0(t)^*$ has the orthogonal decomposition [4] $s_0(t)^* = \gamma_s^* s_0(t) + [\pi_s(1 - |\gamma_s|^2)]^{1/2}s_0'(t)$, where $s_0'(t)$ is an orthogonal component of $s_0(t)$ with $E[s_0(t)s_0'(t)^*] = 0$ and $E[|s_0'(t)|^2] = 1$. Then, the extended observation vector of $\mathbf{x}(t)$ can be rewritten as

$$\tilde{\mathbf{x}}(t) \triangleq [\mathbf{x}(t)^T, \mathbf{x}(t)^H]^T = s_0(t)\tilde{\mathbf{a}}_\gamma + \tilde{\mathbf{v}}_\gamma(t), \tag{4}$$

where $\tilde{\mathbf{a}}_\gamma = [\mathbf{a}_0^T, \gamma_s^*\mathbf{a}_0^H]^T$, $\tilde{\mathbf{v}}_\gamma(t) = [\mathbf{v}(t)^T, \mathbf{v}(t)^H + \mathbf{p}(t)^T]^T$, and $\mathbf{p}(t) = s_0'(t)[\pi_s(1 - |\gamma_s|^2)]^{1/2}\mathbf{a}_0^*$. The optimal WL MVDR beamformer is given by [4]

$$\tilde{\mathbf{w}}_{\text{WL MVDR}} \triangleq [\tilde{\mathbf{a}}_\gamma^H\mathbf{R}_{\tilde{\mathbf{v}}_\gamma}^{-1}\tilde{\mathbf{a}}_\gamma]^{-1}\mathbf{R}_{\tilde{\mathbf{v}}_\gamma}^{-1}\tilde{\mathbf{a}}_\gamma. \tag{5}$$

where $\mathbf{R}_{\tilde{\mathbf{v}}_\gamma} = \langle E[\tilde{\mathbf{v}}_\gamma(t)\tilde{\mathbf{v}}_\gamma(t)^H]\rangle$ is the augmented IPNCM of $\mathbf{x}(t)$. In a practical application, the exact $\mathbf{R}_{\tilde{\mathbf{v}}_\gamma}$ is unavailable and is always replaced by the augmented sample CM $\hat{\mathbf{R}}_{\tilde{x}} = (1/L)\sum_{t=1}^{L}\tilde{\mathbf{x}}(t)\tilde{\mathbf{x}}(t)^H$, where L is the number of snapshots.

3. The Proposed Algorithm

Assuming that the desired signal comes from a direction-of-arrival (DOA) uncertainty region Θ, and no interference comes from this region. Be aware that this assumption has been implemented in [12]. Then, the whole spatial domain Θ_{all} can be divided into two parts, i.e., the angular region of the desired signal Θ and $\bar{\Theta}$, where $\bar{\Theta}$ denotes the complement sector of Θ with $\Theta \cup \bar{\Theta} = \Theta_{all}$ and $\Theta \cap \bar{\Theta} = \emptyset$.

3.1 The Augmented IPNCM Reconstruction

Unlike the IAA algorithm presented in [16], firstly, we use the low-resolution direction finding methods [1] to estimate the interference DOAs in $\bar{\Theta}$. Though there may be some errors in the estimated DOAs, it is certain that the DOAs of all interference always lie in some angular sectors and Θ_k $(k = 1, 2, \cdots, \tilde{K})$ is assumed as the angular sector in which an interference is located. Thus, the interference angular sector can be defined as $\mathbf{\Theta}_i = \Theta_1 \cup \Theta_2 \cup \cdots \cup \Theta_{\tilde{K}}$ $(\tilde{K} \leq K)$, and notice that $\tilde{K} < K$ when two or more interferences are close to each other. Secondly, the interference angular set $\mathbf{\Phi}_i$ and the desired signal angular set $\mathbf{\Phi}_s$ are constructed separately, i.e., $\mathbf{\Phi}_i = [\theta_1^i, \theta_2^i, \cdots, \theta_P^i]$ and $\mathbf{\Phi}_s = [\theta_1^s, \theta_2^s, \cdots, \theta_Q^s]$, where θ_p^i, $p = 1, 2, \cdots, P$ are the sampled angles in $\mathbf{\Theta}_i$, and θ_q^s, $q = 1, 2, \cdots, Q$ are the sampled angles in Θ. Thirdly, let $\mathbf{\Phi} = [\mathbf{\Phi}_i, \mathbf{\Phi}_s]$, then the angular set $\mathbf{\Phi}$ is adopted to obtain the spatial spectrum by using the IAA algorithm. There are two advantages for the process mentioned above. One is that the proposed method has a much lower complexity than the IAA algorithm in [16] since the proposed method has a fewer angular grid points. The other is that it will give us a good estimate of the spatial spectrum even in the presence of the low snapshot numbers, coherent or highly correlated sources [18]. The steps of the IAA algorithm are summarised in Step 2 of the Table 1, where $\mathbf{d}(\theta_n)$ is the array SV corresponding to the direction θ_n, and $\hat{\mathbf{R}}_x = (1/L)\sum_{t=1}^{L}\mathbf{x}(t)\mathbf{x}(t)^H$ is the sample CM of $\mathbf{x}(t)$.

It is easy to see that $\hat{G}_1, \hat{G}_2, \cdots, \hat{G}_P$ are the spatial powers corresponding to the angular set $\mathbf{\Phi}_i$, and $\hat{G}_{P+1}, \hat{G}_{P+2}, \cdots, \hat{G}_{P+Q}$ are the spatial powers corresponding to the angular set $\mathbf{\Phi}_s$. Then, the IPNCM $\tilde{\mathbf{Q}}_r$ and the pseudo IPNCM $\tilde{\mathbf{Q}}_c$ of $\mathbf{x}(t)$ can be reconstructed as

$$\tilde{\mathbf{Q}}_r = \sum_{n=1}^{P}\hat{G}_n\mathbf{d}(\theta_n)\mathbf{d}(\theta_n)^H + \kappa\mathbf{I}, \tag{6}$$

$$\tilde{\mathbf{Q}}_c = \sum_{n=1}^{P}\hat{\gamma}(\theta_n)\hat{G}_n\mathbf{d}(\theta_n)\mathbf{d}(\theta_n)^T, \tag{7}$$

where κ denotes the noise power and can be estimated as the minimum eigenvalue of $\hat{\mathbf{R}}_x$, $\hat{\gamma}(\theta_n) = -\frac{\mathbf{d}(\theta_n)^H\mathbf{E}\mathbf{d}(\theta_n)^*}{\mathbf{d}(\theta_n)^H\mathbf{D}\mathbf{d}(\theta_n)} \cdot \frac{\mathbf{d}(\theta_n)^H\mathbf{d}(\theta_n)}{\mathbf{d}(\theta_n)^H(\mathbf{I}-\hat{\eta}\hat{\mathbf{R}}_x^{-1})\mathbf{d}(\theta_n)}$ is the spatial spectrum of noncircular coefficient corresponding to θ_n [11], [12], $\mathbf{D} \triangleq (\hat{\mathbf{R}}_x - \hat{\mathbf{C}}_x\hat{\mathbf{R}}_x^{*-1}\hat{\mathbf{C}}_x^*)^{-1}$, $\mathbf{E} \triangleq -\mathbf{D}\hat{\mathbf{C}}_x\hat{\mathbf{R}}_x^{*-1}$, $\hat{\mathbf{C}}_x = (1/L)\sum_{t=1}^{L}\mathbf{x}(t)\mathbf{x}(t)^T$, $\hat{\eta}$ is the minimum eigenvalue of $\hat{\mathbf{R}}_{\tilde{x}}$, and $\hat{\mathbf{R}}_{\tilde{x}} = (1/L)\sum_{t=1}^{L}\tilde{\mathbf{x}}(t)\tilde{\mathbf{x}}(t)^H$ is the augmented sample CM of $\mathbf{x}(t)$. Therefore, the augmented IPNCM of $\mathbf{x}(t)$ can be reconstructed as

$$\tilde{\mathbf{R}}_{\tilde{\mathbf{v}}_\gamma} = \begin{bmatrix}\tilde{\mathbf{Q}}_r & \tilde{\mathbf{Q}}_c \\ \tilde{\mathbf{Q}}_c^* & \tilde{\mathbf{Q}}_r^*\end{bmatrix}. \tag{8}$$

3.2 The Desired Signal's Extended SV Estimation

As mentioned above, the augmented signal-plus-noise (SPN) CM $\tilde{\tilde{\mathbf{R}}}_{s+n,\gamma}$ also can be reconstructed as

$$\tilde{\tilde{\mathbf{R}}}_{s+n,\gamma} = \begin{bmatrix}\tilde{\mathbf{R}}_{s+n} & \tilde{\mathbf{C}}_{s+n} \\ \tilde{\mathbf{C}}_{s+n}^* & \tilde{\mathbf{R}}_{s+n}^*\end{bmatrix}, \tag{9}$$

where $\tilde{\mathbf{R}}_{s+n} = \sum_{n=P+1}^{P+Q}\hat{G}_n\mathbf{d}(\theta_n)\mathbf{d}(\theta_n)^H$, $\tilde{\mathbf{C}}_{s+n} = \sum_{n=P+1}^{P+Q}\hat{\gamma}(\theta_n)\hat{G}_n\mathbf{d}(\theta_n)\mathbf{d}(\theta_n)^T$, where $\theta_n \in \mathbf{\Phi}_s, n = (P+1), \cdots, (P+Q)$.

Next, $\tilde{\mathbf{R}}_{\tilde{\mathbf{v}}_\gamma}$ and $\tilde{\tilde{\mathbf{R}}}_{s+n,\gamma}$ can be decomposed as $\tilde{\mathbf{R}}_{\tilde{\mathbf{v}}_\gamma} = \sum_{i=1}^{2N}\lambda_i\mathbf{b}_i\mathbf{b}_i^H$ and $\tilde{\tilde{\mathbf{R}}}_{s+n,\gamma} = \sum_{k=1}^{2N}\delta_k\mathbf{g}_k\mathbf{g}_k^H$, where $\lambda_1 \geq \lambda_2 \geq \cdots \geq \lambda_{2N}$ and $\delta_1 \geq \delta_2 \geq \cdots \geq \delta_{2N}$ are the eigenvalues

Table 1 The steps of the proposed beamforming algorithm.

1. Determine the interference angular sector $\mathbf{\Theta}_i$, then obtain the angular sets $\mathbf{\Phi}_i$ and $\mathbf{\Phi}_s$.

2. Use the IAA algorithm to obtain the spatial spectrum.

Initialize: $\hat{s}_n(t) = [\mathbf{d}(\theta_n)^H\mathbf{x}(t)]/N, \hat{G}_n = (1/L)\sum_{t=1}^{L}|\hat{s}_n(t)|^2$

$\hat{\mathbf{G}} = \mathrm{diag}[\hat{G}_1, \cdots, \hat{G}_{P+Q}], \mathbf{A}(\boldsymbol{\theta}) = [\mathbf{d}(\theta_1), \cdots, \mathbf{d}(\theta_{P+Q})]$

$\{\theta_n \in \mathbf{\Phi}_i, n = 1, \cdots, P\}; \{\theta_n \in \mathbf{\Phi}_s, n = (P+1), \cdots, (P+Q)\}$

Repeat: $\bar{\mathbf{R}} = \mathbf{A}(\boldsymbol{\theta})\hat{\mathbf{G}}\mathbf{A}(\boldsymbol{\theta})^H$

for $n = 1, \cdots, (P+Q)$

$\mathbf{w}_n = \bar{\mathbf{R}}^{-1}\mathbf{d}(\theta_n)/[\mathbf{d}(\theta_n)^H\bar{\mathbf{R}}^{-1}\mathbf{d}(\theta_n)]$, $\hat{G}_n = \mathbf{w}_n^H\hat{\mathbf{R}}_x\mathbf{w}_n$

end for

Until (convergence)

3. Calculate the IPNCM $\tilde{\mathbf{Q}}_r$ according to (6) and the pseudo IPNCM $\tilde{\mathbf{Q}}_c$ according to (7), then reconstruct the augmented IPNCM $\tilde{\mathbf{R}}_{\bar{\mathbf{y}}_\gamma}$ on the basis of (8).

4. Reconstruct the augmented SPNCM $\tilde{\tilde{\mathbf{R}}}_{s+n,\gamma}$ according to (9), then eigen-decompose the matrixes $\tilde{\mathbf{R}}_{\bar{\mathbf{y}}_\gamma}$ and $\tilde{\tilde{\mathbf{R}}}_{s+n,\gamma}$ to get the subspace $\mathbf{U}_{s+i}$.

5. Use the modified AU-IRCB to estimate the desired signal's extended SV.

Initialize: $\bar{\mathbf{a}}_\gamma^0 = [\mathbf{d}(\hat{\theta}_0)^T, \hat{\gamma}(\hat{\theta}_0)^*\mathbf{d}(\hat{\theta}_0)^H]^T$, $\bar{\mathbf{a}}_\gamma = \sqrt{2N}\bar{\mathbf{a}}_\gamma^0/\|\bar{\mathbf{a}}_\gamma^0\|$

Repeat:

5-a. $\beta_a = \left\|\left(\frac{\sqrt{2N}}{\mathbf{U}_{s+i}\mathbf{U}_{s+i}^H\bar{\mathbf{a}}_\gamma} - 2\right)\mathbf{U}_{s+i}\mathbf{U}_{s+i}^H\bar{\mathbf{a}}_\gamma + \bar{\mathbf{a}}_\gamma\right\|^2$

5-b. Calculate $\hat{\bar{\mathbf{a}}}_\gamma$ by solving the following optimization based on the RCB algorithm [19] $\min_{\hat{\bar{\mathbf{a}}}_\gamma} \hat{\bar{\mathbf{a}}}_\gamma^H\hat{\mathbf{R}}_{\tilde{\mathbf{x}}}^{-1}\hat{\bar{\mathbf{a}}}_\gamma$ s.t. $\|\hat{\bar{\mathbf{a}}}_\gamma - \bar{\mathbf{a}}_\gamma\|^2 \le \beta_a$

5-c. Maintain the norm to avoid ambiguity: $\hat{\bar{\mathbf{a}}}_\gamma = \sqrt{2N}\hat{\bar{\mathbf{a}}}_\gamma/\|\hat{\bar{\mathbf{a}}}_\gamma\|$

5-d. Update the presumed SV: $\bar{\mathbf{a}}_\gamma := \hat{\bar{\mathbf{a}}}_\gamma$

5-e. Calculate the new $\tilde{\beta}_a$ from the updated $\bar{\mathbf{a}}_\gamma$ by using the equation in Step *5-a.* Check for convergence: if $\beta_a - \tilde{\beta}_a \le \zeta$, go to Step **6**. Otherwise, go to Step *5-b.*

6. $\tilde{\mathbf{w}}_{pro} = [\hat{\bar{\mathbf{a}}}_\gamma^H\tilde{\mathbf{R}}_{\bar{\mathbf{y}}_\gamma}^{-1}\hat{\bar{\mathbf{a}}}_\gamma]^{-1}\tilde{\mathbf{R}}_{\bar{\mathbf{y}}_\gamma}^{-1}\hat{\bar{\mathbf{a}}}_\gamma$

of $\tilde{\mathbf{R}}_{\bar{\mathbf{y}}_\gamma}$ and $\tilde{\tilde{\mathbf{R}}}_{s+n,\gamma}$, respectively, $\mathbf{b}_i$, $i = 1, \cdots, 2N$ and $\mathbf{g}_k$, $k = 1, \cdots, 2N$ are the corresponding eigenvectors. Then, the interference subspace and the signal subspace can be reconstructed as $\mathbf{U}_i = [\mathbf{b}_1, \mathbf{b}_2, \cdots, \mathbf{b}_{\hat{K}}]$ and $\mathbf{U}_s = [\mathbf{g}_1, \mathbf{g}_2, \cdots, \mathbf{g}_J]$, respectively, where $\hat{K}$ and J are the minimum positive integers which satisfy the expressions $(\sum_{i=1}^{\hat{K}}\lambda_i)/(\sum_{i=1}^{2N}\lambda_i) \ge \xi_1$ and $(\sum_{k=1}^{J}\delta_k)/(\sum_{k=1}^{2N}\delta_k) \ge \xi_2$, respectively, the constants ξ_1 and ξ_2 are used to determine the number of eigenvectors. Thus, the signal-plus-interference (SPI) subspace $\mathbf{U}_{s+i} = [\mathbf{U}_i, \mathbf{U}_s] = [\mathbf{b}_1, \cdots, \mathbf{b}_{\hat{K}}, \mathbf{g}_1, \cdots, \mathbf{g}_J]$.

Inspired by the AU-IRCB algorithm in [17], a modified AU-IRCB is developed to estimate the extended SV of the desired signal. Firstly, we determine the initial desired signal's extended SV by

$$\bar{\mathbf{a}}_\gamma^0 = [\mathbf{d}(\hat{\theta}_0)^T, \hat{\gamma}(\hat{\theta}_0)^*\mathbf{d}(\hat{\theta}_0)^H]^T, \tag{10}$$

where $\hat{\theta}_0$ is the presumed direction of the desired signal. Secondly, a modified AU-IRCB algorithm is developed to estimate the extended SV of the desired signal, and the steps of the modified AU-IRCB algorithm for noncircular signals are summarized in Step **5** of the Table 1, where $\tilde{\mathbf{R}}_{\bar{\mathbf{y}}_\gamma}^{-1} = \begin{bmatrix}\mathbf{D}_{\bar{\mathbf{y}}} & \mathbf{E}_{\bar{\mathbf{y}}} \\ \mathbf{E}_{\bar{\mathbf{y}}}^* & \mathbf{D}_{\bar{\mathbf{y}}}^*\end{bmatrix}$, $\mathbf{D}_{\bar{\mathbf{y}}} = (\tilde{\mathbf{Q}}_r - \tilde{\mathbf{Q}}_c\tilde{\mathbf{Q}}_r^{*-1}\tilde{\mathbf{Q}}_c^*)^{-1}$, $\mathbf{E}_{\bar{\mathbf{y}}} = -\mathbf{D}_{\bar{\mathbf{y}}}\tilde{\mathbf{Q}}_c\tilde{\mathbf{Q}}_r^{*-1}$, and ζ is a specified tolerance. Finally, the proposed beamformer is computed by

$$\tilde{\mathbf{w}}_{pro} = [\hat{\bar{\mathbf{a}}}_\gamma^H\tilde{\mathbf{R}}_{\bar{\mathbf{y}}_\gamma}^{-1}\hat{\bar{\mathbf{a}}}_\gamma]^{-1}\tilde{\mathbf{R}}_{\bar{\mathbf{y}}_\gamma}^{-1}\hat{\bar{\mathbf{a}}}_\gamma. \tag{11}$$

Table 2 The advantages and drawbacks of the proposed method.

Advantages:

1. Not need a priori knowledge of the noncircularity coefficient of the desired signal.
2. Low computational complexity.
3. High output SINRs for the reception of noncircular signals, and maintaining a good performance over a wide range of SINRs.
4. Robust against large DOA mismatch of the desired signal.
5. Can process the coherent interferences.

Drawbacks:

1. Cannot process more interferences than the number of sensors.
2. The angular sector of the desired signal should be a priori, and the interferences must be outside the main beam.
3. Performance degradation for calibration errors.

Throughout the above analysis, our proposed beamforming algorithm has six steps as shown in Table 1.

The main computational complexity of the proposed method is dominated by the following steps: the IAA-based CM reconstruction has a complexity of $O((\mathrm{P}+\mathrm{Q})N^2)$, the extended SV of the desired signal estimation has a complexity of $O(N^3)$, and the computation of $\tilde{\mathbf{R}}_{\bar{\mathbf{y}}_\gamma}^{-1}$ has a complexity of $O(N^3)$. Therefore, the overall complexity of our beamfomer is $\max\{O((\mathrm{P}+\mathrm{Q})N^2), O(N^3)\}$. Compared with the robust WL beamformers in [12]–[15] with complexity equal or higher than $O(N^{3.5})$, the proposed method has a much lower cost especially when N is large.

In order to show the property of the proposed method, the advantages and drawbacks are summarized in Table 2.

4. Simulation Results

In the simulations, a uniform linear array (ULA) with 10 omni-directional sensors spaced half-wavelength distance is considered. The additive noise is modeled as a complex circularly symmetric Gaussian zero-mean spatially and temporally white process. Two interferences are assumed to be from the directions 30° and −50°, respectively. The former one is the BPSK with the noncircularity phase −120°. The latter one is the UQPSK with the noncircularity rate 0.8 and the noncircularity phase −150°. Both their interference-to-noise ratios (INRs) are equal to 30 dB. The presumed direction of the desired signal is $\hat{\theta}_0 = 3°$. The desired signal's angular region is set to be $\Theta = [\hat{\theta}_0 - 8°, \hat{\theta}_0 + 8°] = [-5°, 11°]$, and then $\bar{\Theta} = [-90°, -5°) \cup (11°, 90°]$. The angular sector of the interference is set to be $\mathbf{\Theta}_i = [30° - 8°, 30° + 8°] \cup [-50° - 8°, -50° + 8°] = [22°, 38°] \cup [-58°, -42°]$. For the proposed method, the parameters $\xi_1 = \xi_2 = 0.7$ and $\zeta = 10^{-5}$. The angular sampling interval in the whole spatial domain is 1°. The proposed beamformer is compared with the NC RCB in [10], the Xu's method in [12], and the Huang's method in [15]. The parameters $\varepsilon_a = 0.25N = 2.5$ and $\varepsilon_\gamma = 0.1$ are used in [15]. The parameter $\tilde{\epsilon} = 3$ is used in [10]. The number of snapshots is 50. For achieving the average performance, all the simulation figures are evaluated via 100 Monte Carlo independent runs.

In Fig. 1 and Fig. 2, a scenario with random look di-

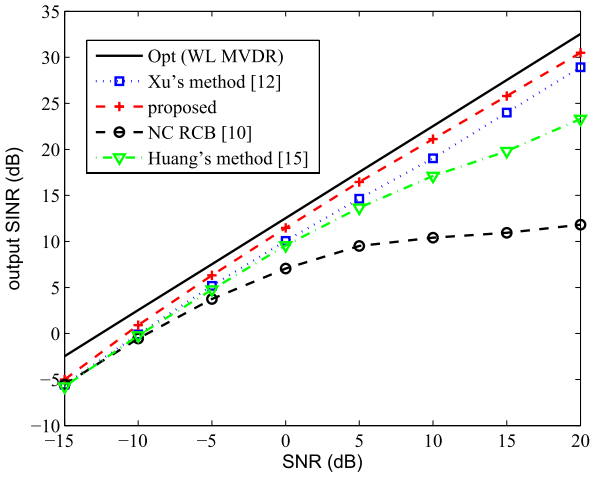

Fig. 1 Output SINR of beamformers versus input SNR in the case of look direction error.

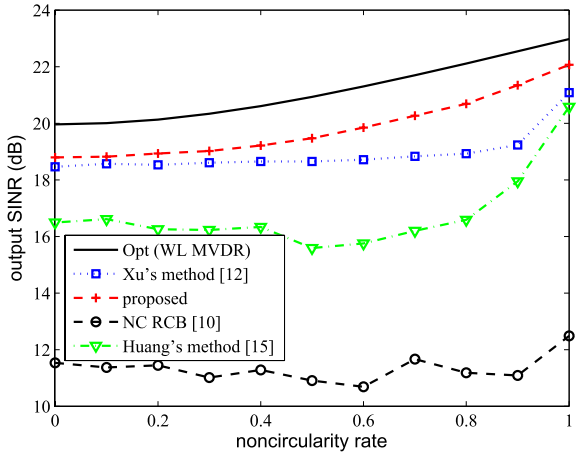

Fig. 2 Output SINR of beamformers versus the noncircularity rate of the desired signal; SNR = 10 dB.

rection mismatch is considered. The desired signal is the UQPSK with the noncircularity rate $|\gamma_s| = 0.9$ and the noncircularity phase $\phi_s = 60°$. The random DOA mismatch of both the desired signal and the interferences are uniformly distributed in $[-4°, 4°]$, i.e., the actual direction of the desired signal θ_0 is uniformly distributed in $[-1°, 7°]$, and the actual directions of the two interferences are uniformly distributed in $[26°, 34°]$ and $[-54°, -46°]$, respectively. Notice that the random DOAs of the desired signal and interferences change from run to run but remain fixed from snapshot to snapshot. According to Fig. 1, when SNR ≤ -10 dB, the performances of all the methods are pretty much the same as each other, when SNR ≥ -5 dB, the proposed method obtains a higher output SINR than the other methods. In addition, the NC RCB suffers severely from performance degradation when SNR ≥ 5 dB.

In Fig. 2, the effect of the desired signal's noncircularity rate on the performance of the four beamformers is studied. The desired signal's noncircularity rate $|\gamma_s|$ varies from 0 to 1 with a step size of 0.1, and the input SNR is fixed at 10 dB. It can be seen from Fig. 2 that the trends of the output SINR curves of the optimal WL MVDR and the proposed method are the same with each other. In addition, the proposed method enjoys the best performance in a large range of the desired signal's noncircularity rate, which indicates that it is robust for both the nonrectilinear signal and the rectilinear signal.

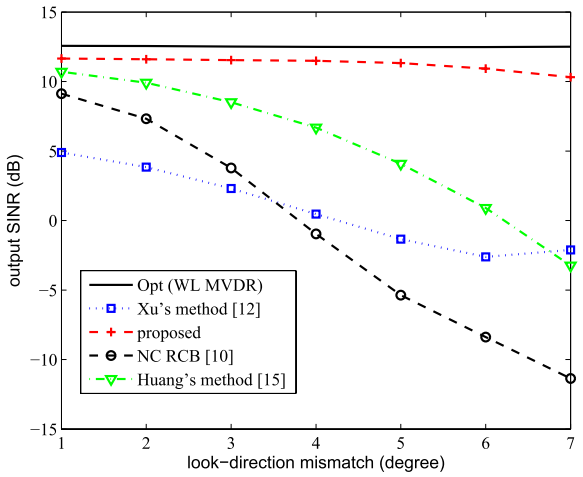

Fig. 3 Output SINR of beamformers versus the look-direction mismatch of the desired signal; SNR = 0 dB.

In Fig. 3, we investigate the performance of all the methods when the look-direction mismatch of the desired signal is increasingly further apart. The simulation conditions in Fig. 3 are the same as Fig. 1 except that the actual direction of the desired signal θ_0 varies from $2°$ to $-4°$ with a step size of $-1°$ (the look-direction mismatch $|\hat{\theta}_0 - \theta_0|$ varies from $1°$ to $7°$), and the DOAs of the two interferences are fixed at $30°$ and $-50°$, respectively. In Fig. 3, we can see that the performance of the proposed beamformer is better than the others over a wide range of look-direction mismatch. Nevertheless, when the look-direction mismatch is greater than $5°$, the performance of the proposed algorithm is shown to be drifted apart from the optimal output SINR due to the error in the extended SV estimation.

In Fig. 4, we consider the scenario that the spatial signature of the desired signal is distorted by coherent local scattering. The desired signal is the UQPSK with the noncircularity rate $|\gamma_s| = 0.9$ and the noncircularity phase $\phi_s = 60°$. The actual desired signal's SV is formed by several signal paths, which can be modeled as $\mathbf{a}_0 = \mathbf{d}(\hat{\theta}_0) + \sum_{k=1}^{4} \exp(j\varphi_k)\mathbf{d}(\theta_k)$, where $\mathbf{d}(\hat{\theta}_0)$ corresponds to the direct path while $\mathbf{d}(\theta_k)$ $(k = 1, \cdots, 4)$ corresponds to the scattered path. φ_k, $k = 1, \cdots, 4$ are uniformly distributed in $[0, 2\pi]$, and θ_k, $k = 1, \cdots, 4$ are independently drawn from a uniform random generator with mean $3°$ and standard deviation $2°$. Notice that φ_k and θ_k change from run to run while remaining constant over snapshots. According to Fig. 4, when SNR ≤ -10 dB, the output SINR of the proposed beamformer is almost the same as the Huang's method, when SNR ≥ -5 dB, the proposed method has the best performance among all the competitors.

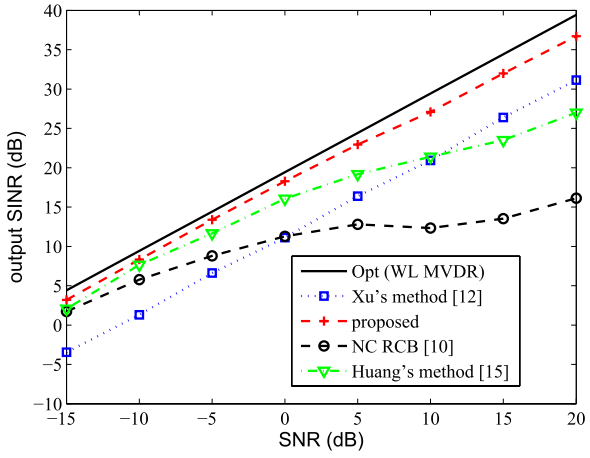

Fig. 4 Output SINR of beamformers versus input SNR in the case of coherent local scattering.

5. Conclusion

In this letter, a new robust WL beamforming algorithm based on the techniques of IAA and AU-IRCB is proposed. The augmented IPNCM is firstly reconstructed and then the presumed SV of the desired signal is corrected to obtain a better performance. The simulation results demonstrate that the proposed beamformer outperforms prior art in both look direction mismatch and coherent local scattering cases.

References

[1] H.L. Van Trees, Optimum Array Processing: Part IV of Detection, Estimation, and Modulation Theory, John Wiley & Sons, 2002.
[2] B. Picinbono, "On circularity," IEEE Trans. Signal Process., vol.42, no.12, pp.3473–3482, 1994.
[3] P. Chevalier and A. Blin, "Widely linear MVDR beamformers for the reception of an unknown signal corrupted by noncircular interferences," IEEE Trans. Signal Process., vol.55, no.11, pp.5323–5336, 2007.
[4] P. Chevalier, J.P. Delmas, and A. Oukaci, "Optimal widely linear MVDR beamforming for noncircular signals," Proc. International Conference on Acoustics, Speech, and Signal Processing, pp.3573–3576, 2009.
[5] P. Chevalier, J.P. Delmas, and A. Oukaci, "Performance analysis of the optimal widely linear MVDR beamformer," Proc. European Signal Processing Conference, pp.587–591, 2009.
[6] P. Chevalier, J.P. Delmas, and A. Oukaci, "Properties, performance and practical interest of the widely linear MMSE beamformer for nonrectilinear signals," Signal Process., vol.97, no.7, pp.269–281, 2014.
[7] Y.M. Shi, L. Huang, C. Qian, and H.C. So, "Shrinkage linear and widely linear complex-valued least mean squares algorithms for adaptive beamforming," IEEE Trans. Signal Process., vol.61, no.1, pp.119–131, 2015.
[8] H. Qian, K. Liu, and W. Wang, "Shrinkage widely linear recursive least square algorithms for beamforming," IEICE Trans. Communications, vol.E99-B, no.7, pp.1532–1540, July 2016.
[9] Y. Xu, J. Ma, Z. Liu, and W. Liu, "A class of diagonally loaded robust Capon beamformers for noncircular signals of interest," Signal Process., vol.94, no.1, pp.670–680, 2014.
[10] F. Wen, Q. Wan, H. Wei, R. Fan, and Y. Luo, "Robust Capon beamforming exploiting the second-order noncircularity of signals," Signal Process., vol.102, no.102, pp.100–111, 2014.
[11] D. Xu, L. Huang, X. Xu, and Z. Ye, "Widely linear MVDR beamformers for noncircular signals based on time-averaged second-order noncircularity coefficient estimation," IEEE Trans. Veh. Technol., vol.62, no.7, pp.3219–3227, 2013.
[12] D. Xu, C. Gong, S. Cao, X. Xu, and Z. Ye, "Robust widely linear beamforming based on spatial spectrum of noncircularity coefficient °C," Signal Process., vol.104, no.6, pp.167–173, 2014.
[13] G. Wang, J.P. Lie, and C.M.S. See, "A robust approach to optimum widely linear MVDR beamformer," Proc. International Conference on Acoustics, Speech, and Signal Processing, pp.2593–2596, 2012.
[14] J. Zhang, L. Huang, L. Zhang, and B. Zhang, "Robust widely linear beamformer based on a projection constraint," Proc. International Conference on Acoustics, Speech, and Signal Processing, pp.2509–2513, 2015.
[15] L. Huang, J. Zhang, L. Zhang, and Z. Ye, "Widely linear minimum dispersion beamforming for sub-Gaussian noncircular signals," Signal Process., vol.122, pp.123–128, 2015.
[16] L. Du, T. Yardibi, J. Li, and P. Stoica, "Review of user parameter-free robust adaptive beamforming algorithms," Digit. Signal Process., vol.19, no.4, pp.567–582, 2009.
[17] J.P. Lie, W. Ser, and C.M.S. See, "Adaptive uncertainty based iterative robust Capon beamformer using steering vector mismatch estimation," IEEE Trans. Signal Process., vol.59, no.9, pp.4483–4488, 2011.
[18] T. Yardibi, J. Li, P. Stoica, and M. Xue, "Source localization and sensing: A nonparametric iterative adaptive approach based on weighted least squares," IEEE Trans. Aerosp. Electron. Syst., vol.46, no.1, pp.425–443, 2010.
[19] J. Li, P. Stoica, and Z. Wang, "On robust Capon beamforming and diagonal loading," IEEE Trans. Signal Process., vol.51, no.7, pp.1702–1715, 2003.